2019 EAGE ANNUAL
81ST CONFERENCE + EXHIBITION
LONDON | THE UNITED KINGDOM

We_R08_02

Enhance Dynamic-Warping for FWI to Mitigate Cycle-Skipping

T. Wang[1]*, Y. Xie[1], M. Wang[1], Y. Guo[1], S. Wu[1], X. Ding[1], S. Wolfarth[2], Y. Supriatna[2], P. Santoso[2]

[1] CGG; [2] BP

Summary

While full waveform inversion (FWI) can provide high resolution velocity models, the method is often let down by the cycle skipping problem. Several solutions based on the estimation of the time shifts have been proposed. Among them, dynamic warping FWI (D-FWI) combines the dynamic warping for the computation of the time shifts between the observed and the predicted data, and a technique which partially warps the observed data to connect the predicted data in a cycle skipping-free way. However, the D-FWI still risks falling into local minima, in particular when the initial model is inaccurate and low-frequency data are missing. Here, we propose a more robust process for estimating the time shifts in which dynamic warping is repeated with offset dependent constraints. The more reliably detected time shifts, can be used in D-FWI with a waveform-based or a traveltime-based objective function to better manage the cycle-skipping problem. We demonstrate the method with a synthetic data from the Marmousi model as well as one challenging OBC dataset from Indonesia.

Introduction

Full waveform inversion (FWI) has been widely used to reconstruct high-resolution velocity model for imaging and interpretation (Sirgue et al., 2009; Ratcliffe et al., 2011). However, classic FWI suffers from the cycle-skipping problem associated with the objective function using the L2-norm of the waveform residual. The success of FWI to recover the low and intermediate wavenumber components of the model highly depends on the long-offset and low-frequency components in the data (Virieux and Operto, 2009). In order to make FWI more robust when starting with a poor initial model and missing low frequency in the seismic data, several approaches involving correlation-based (Van Leeuwen and Mulder, 2010) or deconvolution-based (Warner and Guasch, 2016) misfit criteria have been proposed, following the pioneer work of Luo and Schuster (1991) on wave-equation travel time inversion.

More recently, following a first use of dynamic warping for estimating time shifts for wave-equation reflection traveltime tomography (Ma and Hale, 2013), Wang et al. (2016) proposed an approach called dynamic-warping FWI (D-FWI). In this approach, dynamic warping is used for estimating the time shifts between the observed and the predicted data, and then conventional FWI is performed on a series of partially warped observed data that connect the predicted and the observed data in a cycle skipping-free way (Baek et al., 2014). In this paper, we improve the estimation of the time shifts by an optimized process in which dynamic warping is repeated with offset dependent constraints. Then, as a potential replacement for the conventional FWI performed on a series of partially warped observed data, we also investigate the inversion of a traveltime-based objective function similarly to the recent work of Zhang et al. (2018). We demonstrate the relevance of our method with a synthetic data from the Marmousi model as well as one challenging OBC dataset from Indonesia.

Enhanced dynamic warping

Dynamic warping finds the temporal and spatial varying time shifts by minimizing the least-squares difference between the synthetic and the observed data (Hale, 2013):

$$\tau(\mathbf{x_r},t) = \arg\min_{\tau} \| \mathbf{d}_c(\mathbf{x}_r,t) - \mathbf{d}_o(\mathbf{x}_r,t+\tau(\mathbf{x}_r,t)) \|^2, \tag{1}$$

where $\mathbf{d}_c$ are the synthetic data, $\mathbf{d}_o$ are the observed data and $\mathbf{x}_r$ is the receiver location. The D-FWI method (Wang et al., 2016) mitigates the cycle-skipping by creating a series of bridging datasets $\mathbf{D}_n = \mathbf{d}_o(\mathbf{x}_r,t+\alpha\tau(\mathbf{x}_r,t))$ where $\alpha < 1$ to ensure that there is no cycle-skipping in the least squares cost function:

$$C = \frac{1}{2} \| \mathbf{d}_c - \mathbf{D}_n \|^2 . \tag{2}$$

However, dynamic warping using equation (1) by itself is sensitive to cycle-skipping because if the predicted data match to a totally wrong cycle of the observed data but with close amplitude, dynamic warping is very likely to find a "global minimum" of equation (1), which is not what we want.

To deal with this problem, we propose an enhanced dynamic warping procedure. First, we force the dynamic warping to search along a certain shifting direction to jump out of the unwanted "global minimum" of equation (1). We expect the shifting direction ($\tau > 0$ or $\tau < 0$) smoothly varying with shots and offsets, so that we can create a shot-varying guide by comparing the predicted and the observed data with the selected shots. With this shot-varying guide, the dynamic warping is applied to the data warped by a previous dynamic warping, and this process is repeated several times by searching along the guided direction with a large time window to ensure the solution is not trapped in the unwanted "global minimum". During this searching process, an offset dependent constraint fixes the searched value within a reasonable range:

$$|\tau(\mathbf{x}_r,t)| < S(\mathbf{x}) = \begin{cases} a, (0,x_1) \\ b, (x_1,x_2) \\ c, (x_2,\infty) \end{cases}, \tag{3}$$

in which x_1 and x_2 are different offsets and $S(\mathbf{x})$ is an offset-dependent function where the value a, b and c

are the thresholds which are determined based on the comparison of the synthetic and the observed diving waves. Finally, we apply a series of conventional dynamic warping with a small searching window to fine tune and detect the accurate time shifts by allowing searching along both positive and negative directions. This enhanced dynamic warping procedure makes the estimation of the time shifts reliable and hence the results of D-FWI more robust. Moreover, the cost function of a L2-norm of traveltime differences:

$$C_\tau = \frac{1}{2} \parallel \tau(\mathbf{x}_r, t) \parallel^2, \tag{4}$$

even more stabilizes the optimization process (Luo and Schuster, 1991; Zhang et al., 2018). The above objective function mitigates the mismatch of amplitudes and is more convex to overcome the cycle-skipping problem even starting with a relatively higher frequency.

Applications

We first apply the above described enhanced D-FWI to a modified Marmousi model. As shown in Figure 1(a), a 200 m thick water layer is added on the top of the original model. 200 shots are evenly placed at the depth of 24 m with an interval of 48 m. The receiver interval is 24 m and also deployed at the depth of 24 m. The free surface is used to simulate the ghost and multiples. The maximum offset for FWI is 9 km. We start from the laterally invariant initial model with a correct water velocity as shown in Figure 1(b).

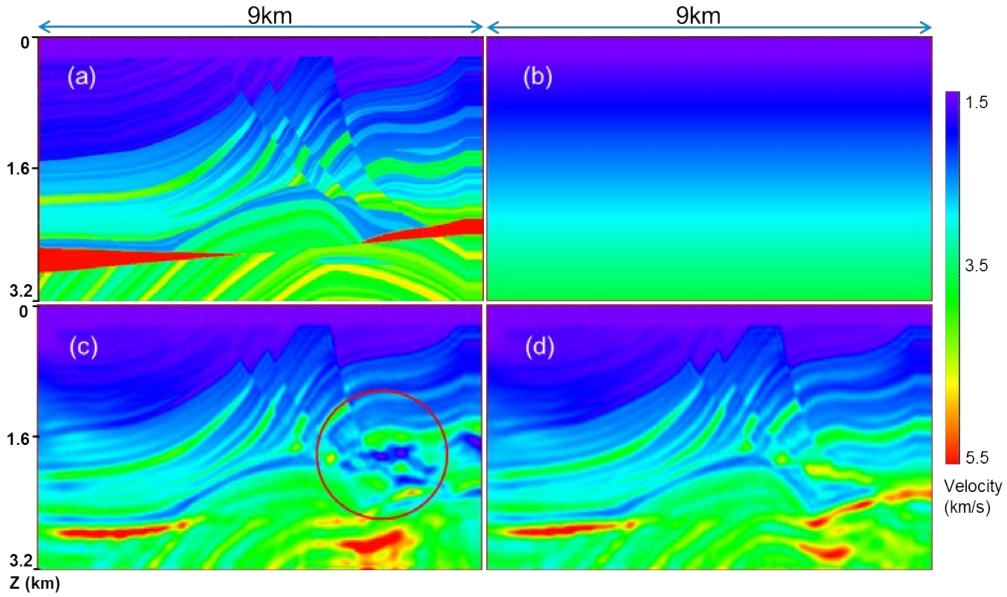

Figure 1 *(a) The Marmousi model with an additional 200 m water layer. (b) Laterally invariant initial model with a correct water velocity. (c) Result from standard D-FWI from 5 Hz to 10 Hz. (d) Result from enhanced D-FWI from 5 Hz to 10 Hz. We can see that enhanced D-FWI successfully recovers the correct model on the right-bottom part, while the standard D-FWI converges to a local minimum.*

To demonstrate its effectiveness, we compare the proposed enhanced D-FWI with the standard D-FWI. The iteration scheme is the same for both tests: using only the diving wave part with a limited offset of 6 km for 40 iterations at 5 Hz, followed by the use of diving waves with all offsets for another 40 iterations at 5 Hz. Finally, we switch back to the conventional FWI using all of the data (diving wave, reflections and multiples) from 5 Hz to 10 Hz. As Figure 1(c) shows, the standard D-FWI gives a relatively good result except for the deep part on the right hand side. This is due to the complexity of the fault area and the standard D-FWI fails to recover the background velocity without enough low frequency data. In comparison, the enhanced D-FWI gradually reconstructs the background information after using the time shift-based objective function cascaded by the waveform-based objective function. Based on that, the conventional waveform-based FWI can converge to the correct model.

We then applied our proposed enhanced D-FWI method to an OBC field data from Indonesia. The shot spacing is 50x100 m while the receiver spacing is 50x500 m with a maximum offset of 9.6 km. The low frequency component of this dataset is quite noisy due to the very shallow water depth and the outdated cables used during the acquisition. It is difficult to build a good initial model using tomography, because the top of the carbonate layer is very shallow and there are no useful reflections inside the layer. Here, the initial model is a direct extension of the model according to the horizons from the neighbouring survey. We can see the obvious inconsistency between the velocity and geological structure from the depth slice (area inside the rectangle in Figure 2(d)). According to the synthetic shot QC, we observe that the velocity in the shallow carbonate layer is too slow to match the real data. The conventional FWI and the standard D-FWI failed to update the model as the inversion is severely cycle-skipped with this initial model.

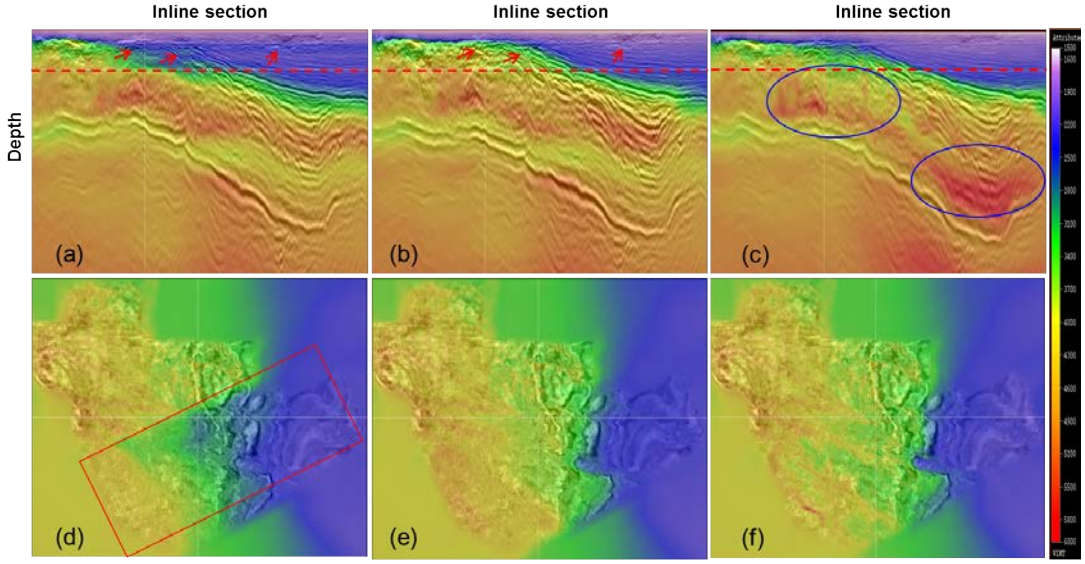

Figure 2 *The real data example from Indonesia. (a) The initial model, (b) Enhanced D-FWI model after 4 Hz to 6 Hz update, (c) Final model based on (b) after conventional high frequency FWI and tomography, (d), (e) and (f) are the depth slices (indicated by the red dash line) corresponding to (a), (b) and (c), respectively. The rectangle in (d) indicates the update area of this dataset.*

We apply the enhanced D-FWI from 4 Hz to 6 Hz using a maximum offset of 4 km at first and then we include all offsets for inversion. The enhanced D-FWI gradually heals the slow velocity around the top of carbonate and removes the high velocity layer in the shallow on the right-hand side, as indicated by the red arrow in Figure 2(b). On the depth slices, we can see that the velocity model is more consistent with the geology after the enhanced D-FWI. Since the time shift-based objective function is used during the enhanced D-FWI, the result is a smooth update which needs further updates to improve the resolution. By cascading with conventional FWI up to 8 Hz and joint tomography combining the first breaks and residual moveouts in the CIGs (Allemand et al., 2017), we get updated models which are overlaid on the corresponding migration results in Figure 2(c). The conventional FWI adds detailed velocity variations delineating the faults in the carbonate layer. The right-bottom part beyond the diving wave penetration is updated by tomography. In Figure 3, we can see the structure is improved and CIGs are flattened with the final velocity model. In the crossline section, the undulations are removed on the final migration result which shows a more reasonable geological structure than the result using the initial model.

Conclusions

We have developed enhanced D-FWI which employs an optimized dynamic warping procedure to better mitigate the cycle-skipping problem. We estimate the traveltime differences of the diving waves, and then with either a time shift-based or a waveform misfit-based objective function, we can recover the background velocity model while conventional FWI suffers from cycle-skipping. The presented synthetic and real data examples demonstrate the effectiveness of our enhanced D-FWI for overcoming the

cycle-skipping problem.

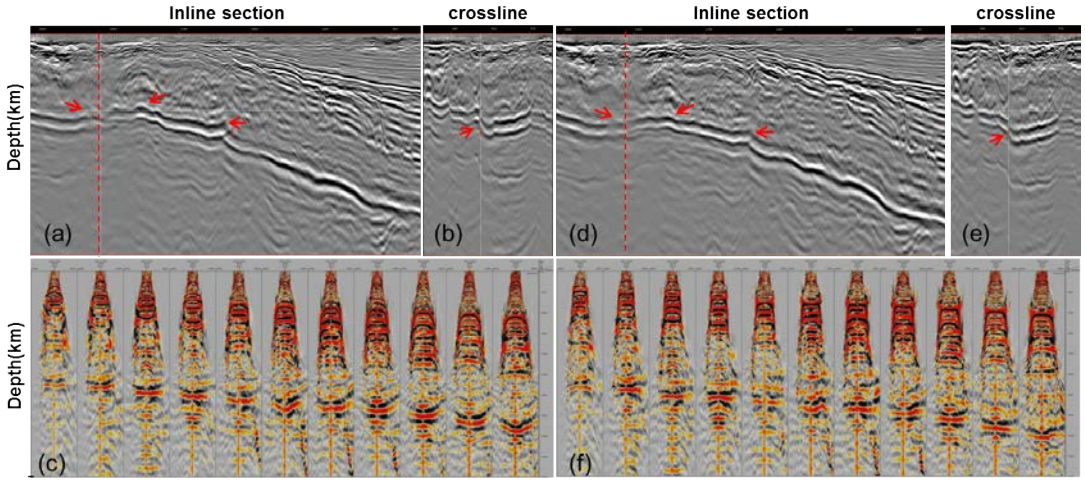

Figure 3 *The 3D depth migration result of initial model (a, b, c) and final velocity model (d, e, f): (a) and (d) The inline section, (b) and (e) The crossline section located the at red dash line, (c) and (f) CIGs of the inline section in (a) and (d).*

Acknowledgements

The authors would like to thank BP and CGG for permission to show this work; thank SKK Migas and DitJen Migas for permission to publish.

References

Allemand, T., Sedova, A. and Hermant, O. [2017] Flattening common image gathers after full-waveform inversion: The challenge of anisotropy estimation. *SEG Technical Program Expanded Abstracts 2017*, 1410–1415.

Baek, H., Calandra, H. and Demanet, L. [2014] Velocity estimation via registration-guided least-squares inversion. *Geophysics*, **79**(2), R79–R89.

Hale, D. [2013] Dynamic warping of seismic images. *Geophysics*, **78**(2), S105–S115.

Luo, Y. and Schuster, G.T. [1991] Wave-equation traveltime inversion. *Geophysics*, **56**(5), 645–653.

Ma, Y. and Hale, D. [2013] Wave-equation reflection traveltime inversion with dynamic warping and full-waveform inversionWERTI with dynamic warping. *Geophysics*, **78**(6), R223–R233.

Ratcliffe, A., Win, C., Vinje, V., Conroy, G., Warner, M., Umpleby, A., Stekl, I., Nangoo, T. and Bertrand, A. [2011] Full waveform inversion: A North Sea OBC case study. *SEG Technical Program Expanded Abstracts 2011*, 2384–2388.

Sirgue, L., Barkved, O., Van Gestel, J., Askim, O. and Kommedal, J. [2009] 3D waveform inversion on Valhall wide-azimuth OBC. *71st EAGE Conference and Exhibition incorporating SPE EUROPEC 2009*.

Van Leeuwen, T. and Mulder, W. [2010] A correlation-based misfit criterion for wave-equation traveltime tomography. *Geophysical Journal International*, **182**(3), 1383–1394.

Virieux, J. and Operto, S. [2009] An overview of full-waveform inversion in exploration geophysics. *Geophysics*, **74**(6), WCC1–WCC26.

Wang, M., Xie, Y., Xu, W.Q., Loh, F.C., Xin, K., Chuah, B.L., Manning, T. and Wolfarth, S. [2016] Dynamic-warping full-waveform inversion to overcome cycle skipping. *SEG Technical Program Expanded Abstracts 2016*, 1273–1277.

Warner, M. and Guasch, L. [2016] Adaptive waveform inversion: Theory. *Geophysics*, **81**(6), R429–R445.

Zhang, Z., Mei, J., Lin, F., Huang, R. and Wang, P. [2018] Correcting for salt misinterpretation with full-waveform inversion. *SEG Technical Program Expanded Abstracts 2018*, 1143–1147.